An AIE fungal vacuole membrane probe toward species differentiation, vacuole formation visualization, and targeted photodynamic therapy

Bingnan Wang [a,b,d], Siyuan Wang [c], Chunyang Li [a,b], Jianqing Li [a,b], Meixi Yi [a,b], Jing-Wen Lyu [e], Bing Gu [e], Ryan T.K. Kwok [d], Jacky W.Y. Lam [d], Anjun Qin [a,b,*], Ben Zhong Tang [b,c,d,**]

[a] State Key Laboratory of Luminescent Materials and Devices, Guangdong Provincial Key Laboratory of Luminescence from Molecular Aggregates, South China University of Technology, Guangzhou, 510640, China
[b] Center for Aggregation-Induced Emission, South China University of Technology, Guangzhou, 510640, China
[c] School of Science and Engineering, Shenzhen Institute of Aggregate Science and Technology, The Chinese University of Hong Kong, Shenzhen, (CUHK-Shenzhen), 518172, China
[d] Hong Kong Branch of Chinese National Engineering Research Centre for Tissue Restoration and Reconstruction, Department of Chemistry, The Hong Kong University of Science & Technology, Clear Water Bay, Kowloon, 999077, Hong Kong, China
[e] Department of Clinical Laboratory Medicine, Guangdong Provincial People's Hospital (Guangdong Academy of Medical Sciences), Southern Medical University, Guangzhou, 510000, China

ARTICLE INFO

ABSTRACT

Vacuoles are unique organelles of fungi. The development of probes targeting the vacuoles membrane will enable visualization of physiological processes and precise diagnosis and therapy. Herein, a zwitterionic molecule, MXF-R, comprising of an aggregation-induced emission (AIE) photosensitizing unit and an antibiotic moxifloxacin, was found capable of specifically imaging vacuole membrane and using for targeted antifungal therapy. MXF-R demonstrated a higher signal-to-noise ratio, stronger targeting capability, and better biocompatibility than the commercial probe FM4-64. By using MXF-R, real-time visualization of vacuole formation during *Candida albicans* (*C. albicans*) proliferation was achieved. More importantly, owing to its varying staining ability towards different fungus, MXF-R could be used to quickly identify *C. albicans* in mixed strains by fluorescence imaging. Moreover, MXF-R exhibits a remarkable ability to generate reactive oxygen species under white light, effectively eradicating *C. albicans* by disrupting membrane structure. This antifungal therapy of membrane damage is more effective than clinical drug fluconazole. Therefore, this work not only presents the initial discovery of a probe targeting vacuolar membrane, but also provides a way to develop novel materials to realize integrated diagnosis and therapy.

1. Introduction

Fungal infections will lead to a range of diseases such as aspergillosis, septicemia, and meningitis, presenting a significant threat to human health [1]. In clinical practice, the diagnosis of fungal infections usually requires the culture and strain identification of microbial samples, which takes a relatively long time. The fast replication of fungi through asexual reproduction often results in the swift deterioration of the diseases. Moreover, in the treatment of fungal infections, antibiotics are the primary approach, but it's very difficult to completely eradicate fungi.

Long-term use of antibiotics is required to inhibit the growth of fungi, but prolonged usage of antibiotics would lead to the drug resistance [2,3]. Therefore, rapid fungal infections diagnosis and effective treatment are two crucial research subjects in clinical practice [4–12].

The fungal vacuole serves as a distinctive organelle response for storing enzymes, amino acids and nutrients, regulating osmotic pressure, and performing lysosomal functions. The form, number, and size of vacuoles vary with the morphology and age of the fungus [13]. Moreover, vacuoles are typically present in mature fungus and serve as crucial indicators of different phenotype [14]. The development of

targeted fungal vacuole membrane probes that can visualize the location, distribution and dynamic changes of vacuoles, is highly important because it enables rapid differentiation of fungal species through vacuole membrane staining and thus realize the diagnosis of fungi. More importantly, compared with antibiotics, which could easily lead to resistance, the treatment which destroyed the membrane structure will be more effective and less resistant [15–18]. However, the current development of targeted fluorescent probes predominantly focuses on cells with relatively few reports on fungal organelles [19–25]. Furthermore, fewer studies have been reported on the internal vacuole membrane, because the similar membrane structure of the vacuolar membrane and the outer cell membrane makes it difficult to distinguish accurately. At present, fungal vacuoles could be labeled with commercial cell membrane probes because of their monolayer membrane structures. These probes such as FM4-64 often feature two-ion salt components with pyridine salt and quaternary ammonium salt [26]. Nonetheless, certain limitations exist with these probes, including poor specificity, altering fungal activity, low signal-to-noise ratio, aggregation-caused quenching (ACQ) effect, single function, expensive and so on (Fig. 1A). To address these challenges, the development of alternative fluorescent probes targeting membrane structures necessitates the exploration of novel strategies.

Notably, targeting has always been a difficult problem in the process of fluorescent probes discoveries [27,28]. It is mainly because the targeted molecules are quite limited, and their targeting ability will be greatly reduced or even ineffective after the targeted molecules are attached to fluorescent probes [29,30]. Moreover, for some targeting probes, their targeting mechanism is not clear, which is difficult to guide further development of such probes. Drugs have been widely recognized as targeted molecules. The combination of drugs and fluorescent molecules to prepare targeted probes has proved to be an effective strategy [31]. For example, the commercial endoplasmic reticulum (ER) dye ER-Tracker Green achieved targeted imaging by linking glibenclamide and BODIPY derivatives.

Our group has been committed to the selective imaging and killing of microorganisms [32–35]. In our previous work, we studied the optical properties and structure-activity relationships of the antibiotic moxifloxacin (MXF) and developed functionalized MXF derivatives for the diagnosis and treatment [30,35], which have the advantages of fast identification of microorganisms and are not easy to produce drug resistance. In addition to being a clinical antibiotic against bacteria, MXF has also been found to inhibit fungi through multitargeting [36]. As a microorganism with more complex structure than bacteria, the rapid diagnosis and effective treatment of fungi is a challenge in clinical practice.

Occasionally, we found MXF-R, comprising of an AIE photosensitizing unit and an antibiotic MXF, showed a remarkable ability to target the vacuolar membrane of fungi (Fig. 1A). However, its AIEgen of DMAPy can only target mitochondria (Fig. S1). The targeting capability of MXF-R enables visualization of the in-situ vacuole formation process
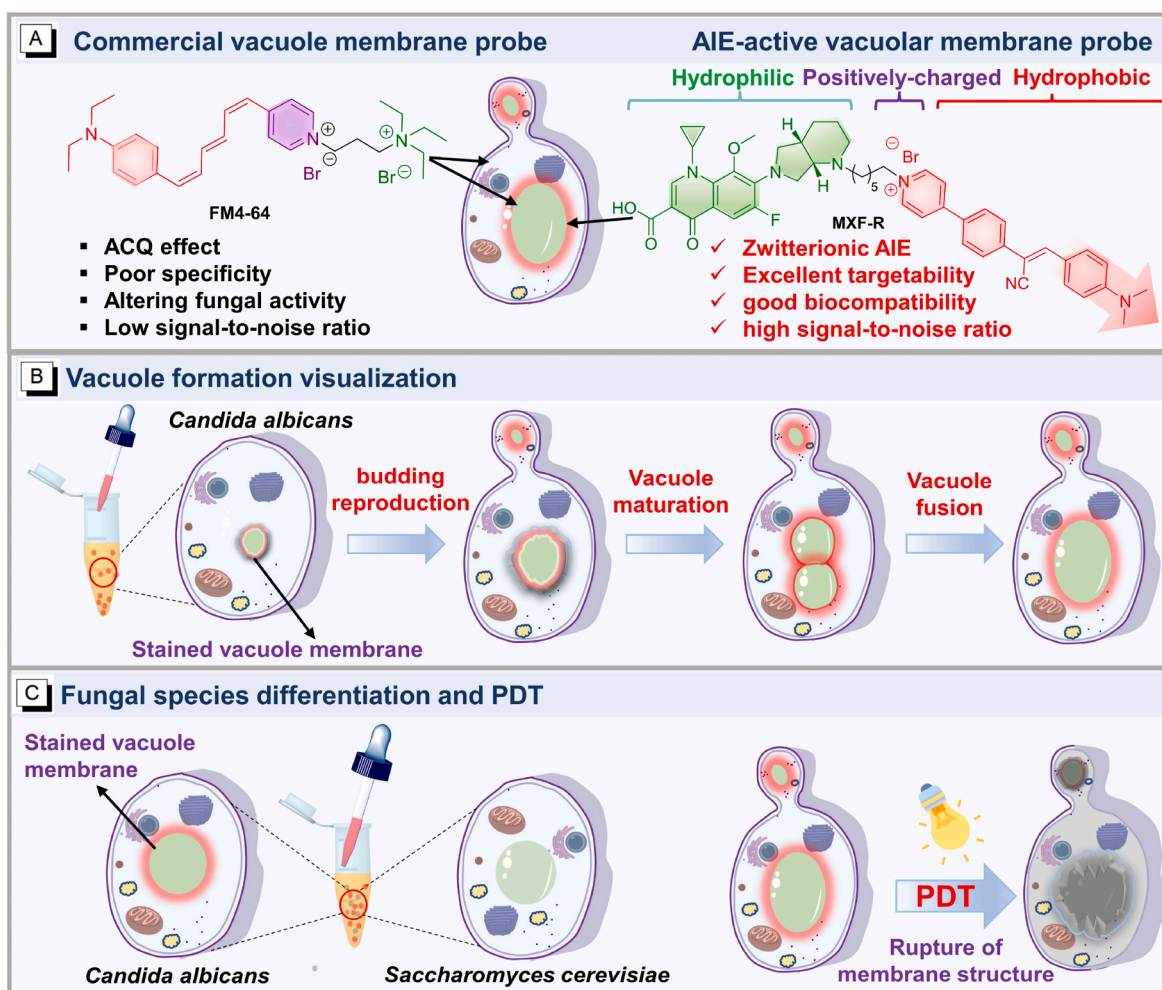

Fig. 1. Design of AIE-active vacuolar membrane probe and biological applications. (A) Disadvantages of commercial vacuole membrane probe FM4-64 and advantages of AIE-active vacuolar membrane probe MXF-R. (B) Visualizing the proliferation of *Candida albicans* using MXF-R. (C) The fungal species differentiation and photodynamic antifungal therapy of MXF-R.

during the proliferation of *C. albicans* (Fig. 1B), which encouraged us to conduct a comprehensive analysis to study its underlying mechanism. It is worth noting that MXF-R exhibited higher signal-to-noise ratio, and better biocompatibility than FM4-64. By leveraging the differential staining ability of MXF-R for different funguses, we successfully identified various types of funguses. In addition, ROS production ability of MXF-R was harnessed to effectively eliminate *C. albicans*, surpassing the efficacy of the commercial antibiotic fluconazole (Fig. 1C). This study not only identifies a novel fluorescent probe that target the vacuole membrane with high efficiency, but also paves a way for the development of the probes for the integrated rapid diagnosis and treatment of fungal infections.

2. Materials and methods

2.1. Materials

All chemicals and reagents were purchased from commercial companies and used without further purification. Phosphatidyl ethanolamine (POPE) and 1-palmitoacyl-2-oleyl lecithin (POPC) were purchased from Energy Chemical. FM4-64 and fluconazole were purchased from aladdin. DMEM (Dulbecco's modified Eagle medium) and fetal bovine serum (FBS) were purchased from Termo Fisher Scientific (Shanghai, China). HeLa cells were obtained from cell culture center of Institute of Basic Medical Sciences, Chinese Academy of Medical Science (Beijing, China). *Saccharomyces cerevisiae* and *Candida albicans* were obtained from China General Microbiological Culture Collection Center. *Candida tropicalis, Candida parapsilosis, Candida glabrata, Aspergillus fumigatus, Aspergillus niger, Aspergillus flavus* and *Aspergillus terrestris* were obtained from Guangdong Provincial People's Hospital.

2.2. Culture and staining of funguses

A single fungal colony on a solid agar plate was transferred to 10 mL liquid yeast extract peptone dextrose (YPD) medium and cultured at 30 °C or 37 °C (*Saccharomyces cerevisiae, Candida albicans, Candida tropicalis, Candida parapsilosis* and *Candida glabrata* cultured at 30 °C are yeast morphologies, while these fungi cultured at 37 °C are pseudohyphal or mycelium morphologies) for 10 h. *Aspergillus fumigatus, Aspergillus niger, Aspergillus flavus* and *Aspergillus terrestris* were cultured in YPD medium at 30 °C for 3 days. Funguses were harvested by centrifugation (7100 rpm, 2 min) and washed with PBS solution for 3 times. The supernatant was removed and fungi was suspended in PBS, and diluted to an optical density of 2.0 at 600 nm ($OD_{600} = 2.0$).

2.3. Fungal staining and imaging

The fungi solution (100 μL, $OD_{600} = 2.0$) was added to 900 μL PBS solution containing MXF-R or DMAPy to produce the mixture with the concentration of 10 μM. Then the mixture was incubated at 37 °C for certain times. The fungi were harvested by centrifuging (7100 rpm for 2 min) and re-suspended in 30 μL PBS. 5 μL fungal solution was added to the glass slides, and covered with a coverslip to fix fungi. The samples were imaged using confocal laser scanning microscopy (CLSM). The excitation wavelength of DMAPy and MXF-R was 488 nm.

2.4. Visualization of fungal proliferation process

The *C. albicans* was stained using MXF-R according to the fungal staining method. The *C. albicans* were harvested by centrifugation (7100 rpm for 2 min) and re-suspended in 1 mL YPD medium. The *C. albicans* solution was added to a covered petri dish with a coverslip to fix *C. albicans*. In the online culture system of CLSM, the *C. albicans* were cultured at 37 °C to observe the proliferation by imaging.

2.5. Fungal viability and photodynamic killing

Various concentrations of FM4-64, MXF-R or DMAPy were incubated with *C. albicans* ($OD_{600} = 0.2$) in PBS solutions. For the photodynamic group, after incubated for 20 min, the mixed *C. albicans* suspension was irradiated for 30 min under white light (90 mW/cm^2). For the group without irradiation, the *C. albicans* suspension was incubated for 50 min. These *C. albicans* suspensions were serially diluted 500 times with PBS. *C. albicans* suspension (100 μL) was dripped into the agar plate and then dispersed evenly by the spreader. After *C. albicans* of agar plates were incubated at 37 °C for 24 h, the colonies were counted.

Fungal viability (%) was calculated as following:

Fungal viability = $C/C_0 \times 100\%$;

where C is the CFU of the experimental group treated by in FM4-64, MXF-R or DMAPy, and C_0 is the CFU of the PBS group.

2.6. Analysis of reactive oxygen species in funguses

DCFH-DA was used as an indicator to detect the production of reactive oxygen species in fungi. After 500 μM N-acetyl-L-cysteine (NAC) or 10 μM DCFH-DA was incubated with *C. albicans* ($OD_{600} = 0.2$) in PBS solution at 37 °C for 1 h. MXF-R (stock solution: 10 mM in DMSO) were added to the fungal suspensions to produce the solution with the concentration of 10 μM. For the white light irradiation group, after incubated for 20 min, the fungal suspensions were exposed to white light (90 mW/cm^2) for 5 min. Whereas that without white light irradiation, the fungal suspensions were incubated for 25 min. Fungi were harvested by centrifuging and re-suspended in 30 μL of PBS. The stained fungal solution (5 μL) was added to glass slides, and then covered with a coverslip to fix fungi. The samples were observed by CLSM. The excitation wavelength was 488 nm. The fluorescence signal of indicator was monitored in a range of 500–550 nm.

2.7. Scanning electron microscopy (SEM) analysis

First, *C. albicans* ($OD_{600} = 0.2$) were incubated in PBS solution at 37 °C under different treatment conditions. For the white light irradiation group, after incubated for 20 min, the fungal suspensions were exposed to white light (90 mW/cm^2) for 30 min, and that without white light irradiation, the fungal suspensions were incubated for 50 min. Next, the fungi were washed three times with PBS and then fixed with 3 % glutaraldehyde overnight. Afterward, the fungi were washed five times with PBS and then dehydrated with 20 %, 40 %, 60 %, 70 %, 80 %, 90 %, 95 % and 100 % ethanol in sequence over 10 min the *C. albicans* suspensions were dropped on the silicon chip for natural evaporation to make the samples. Finally, the samples were sprayed by gold and photographed by SEM.

3. Results and discussion

3.1. Photophysical properties of MXF-R

MXF-R were synthesized according to our reported methods by attaching DMAPy to the secondary amine part of MXF [35]. Next, the photophysical properties of MXF-R in PBS containing 1 % DMSO before and after binding with *C. albicans* were characterized. As shown in Fig. 2A, the maximum absorption peak of MXF-R was recorded at 462 nm. After addition of *C. albicans* ($OD_{600} = 2.0$), the wavelength did not show significant change, indicating that *C. albicans* only had very slight effect on the absorption wavelength of MXF-R. Furthermore, the photoluminescence (PL) spectra of the MXF-R in PBS solution containing 1 % DMSO before and after binding with *C. albicans* were also tested. In the absence of *C. albicans*, the PL intensity of MXF-R were weak. However, after addition of *C. albicans*, its PL intensity was obviously
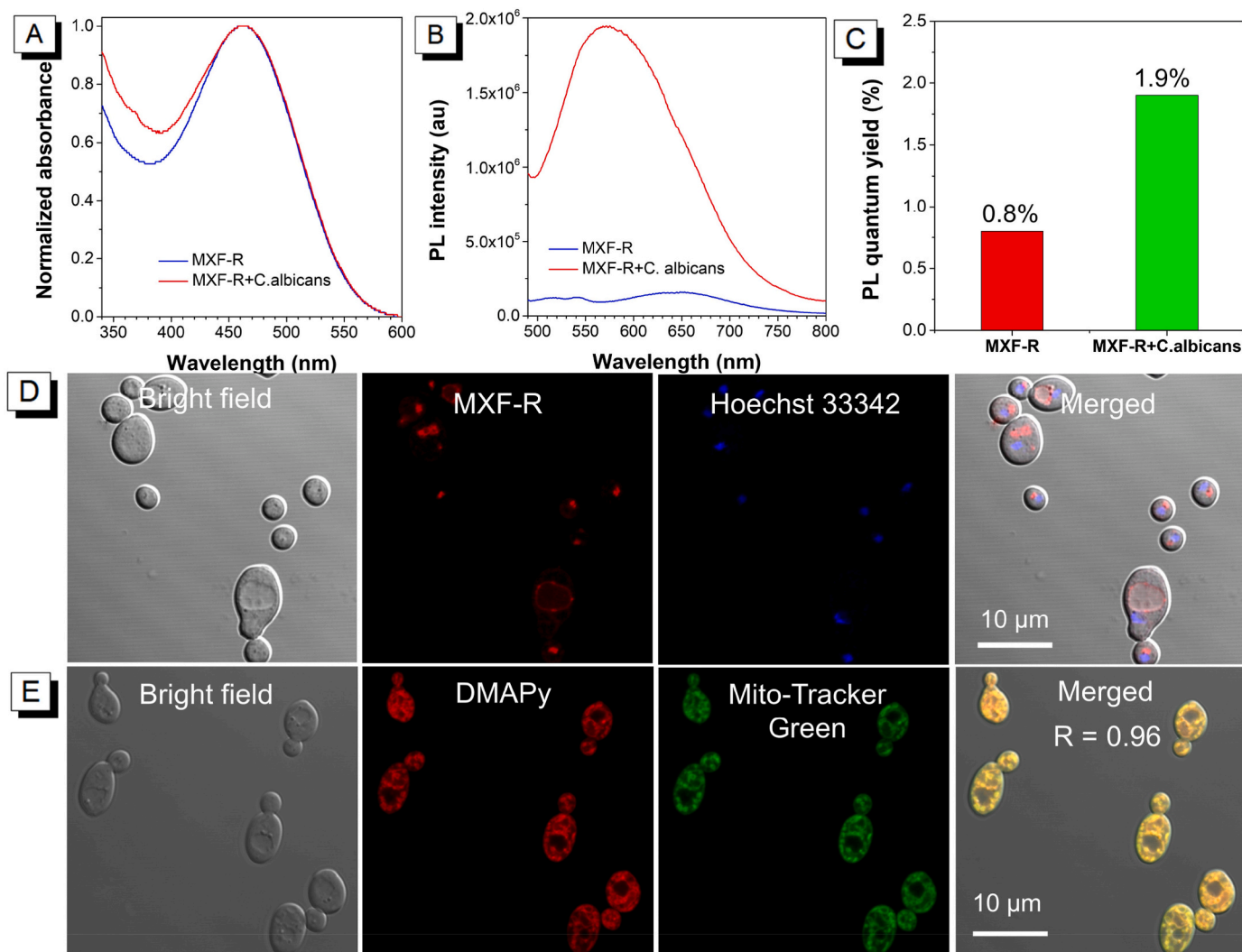
Fig. 2. (A) Normalized absorption spectra of MXF-R in PBS solution containing 1 % DMSO before and after addition of *C. albicans*. (B) PL spectra of MXF-R in PBS solution containing 1 % DMSO before and after addition of *C. albicans*. (C) The absolute PL quantum yield of MXF-R in PBS solutions containing 1 % DMSO before and after addition of *C. albicans*. The OD_{600} value of *C. albicans* was 2.0. (D) Fluorescent photographs of *C. albicans* stained with MXF-R and Hoechst 33342. (E) Fluorescent photographs of *C. albicans* co-stained with DMAPy and Mito-Tracker Green and the pearson's correlation coefficients (R) was 0.96; Concentration: 10 μM. (For interpretation of the references to colour in this figure legend, the reader is referred to the Web version of this article.)

strengthened and the emission wavelength was blue-shifted (Fig. 2B). This might be attributed to the decrease in the polarity of the environment around the molecules after MXF-R binds to *C. albicans*. To accurately show the PL changes, the absolute PL quantum yields of MXF-R solutions were characterized before and after binding with *C. albicans*, which increased from 0.8 % to 1.9 % (Fig. 2C). The restriction of intramolecular motions of MXF-R after binding with *C. albicans* could be the main reason of the enhanced PL quantum yields. To further validate this hypothesis, we conducted PL spectra of MXF-R at varying glycerol concentrations (Fig. S2). The results indicated a progressive enhancement in its PL intensity as the glycerol concentration increased because of the restriction of intramolecular motion. In addition, the stability of MXF-R was analyzed under different pH conditions by high performance liquid chromatography, and the results showed that it remained intact in buffer solutions at pH 5.5, 7.4 and 9.0 (Fig. S3), which laid the foundation for the potential use of MXF-R in bioimaging and therapeutic applications.

3.2. Location distribution of molecules in C. albicans

Thanks to its AIE feature, we further explored the distribution of

MXF-R in *C. albicans*. For comparison, DMAPy, and the DNA fluorescent dye Hoechst 33342 were also used. As shown in Fig. 2D and S4, the location of the nucleus was labeled with the blue fluorescent dye Hoechst 33342. DMAPy was mainly distributed outside the nucleus and filled with the entire *C. albicans*, while MXF-R was attached to dot or circle structures. By analyzing the structure of the fungus [13,14], those circles and dots are the vacuolar membranes and their precursors. Next, fluorescent co-localization imaging experiments were performed using DMAPy and mitochondrial dye Mito-Tracker Green. The results showed that they were highly overlapped and the Pearson's correlation coefficient (R) up to 0.96 (Fig. 2E), which might be attributed to the electrostatic adsorption of the positively charged DMAPy with the negatively charged mitochondria. To elucidate the distinct staining characteristics of DMAPy and MXF-R, the zeta potentials were recorded, which demonstrated that the latter had a lower positive charge than the former (Fig. S5). This is because the carboxylic acid group in the MXF moiety of MXF-R neutralizes a portion of the positive charge. In addition, we speculate that the larger steric hindrance of MXF may increase the residence time of MXF-R on the membrane. Therefore, the MXF unit in MXF-R plays a very important role for this targeting behavior.

3.3. Fluorescent imaging of MXF-R and FM4-64

Next, the fluorescent imaging effect of MXF-R and FM4-64 on the vacuolar membranes of *C. albicans* was compared. As shown in Fig. 3A–C, FM4-64 not only stained the vacuolar membrane, but also the residues on the outer plasma membrane of the fungus. Meanwhile, the intensity profile of synchrony for linear analysis showed that the fluorescence intensity of FM4-64 on the vacuolar membrane was 1.3–3.9 times higher than that on the plasma membrane (Fig. 3B and C). In contrast, the fluorescence intensity of MXF-R on the vacuolar membrane was 4.8–8.9 times higher than that on the plasma membrane (Fig. 3D–F). This could be attributed to the binding of MXF-R to the vacuolar membrane, which led to the restriction of intramolecular motion and thus enhanced fluorescence intensity. These results confirmed that MXF-R possessed higher signal-to-noise ratio in staining vacuolar membrane than that of FM4-64. In addition, fluorescent staining experiments of MXF-R and FM4-64 were performed on *C. albicans* of pseudohyphal morphologies. It was found that MXF-R remained less on the plasma membrane and surpassingly stained the internal vacuolar membrane (Fig. 3G). However, FM4-64 was mainly distributed in the plasma membrane (Fig. 3H). The results revealed that MXF-R showed excellent staining effect on the vacuolar membrane of fungi, and superior over FM4-64.

3.4. Theoretical simulation of targeting membrane capability

To reveal the reason of the specific staining of vacuolar membranes by MXF-R, its function was analyzed. For comparison, MXF and DMAPy were also used. First, the octanol-water partition coefficient (logP) of MXF, MXF-R, DMAPy was tested by the shake-flask method. The results showed that logP of MXF, MXF-R and DMAPy were −1.486, −0.790, and 0.927, respectively, indicating that their hydrophobicity was gradually increased (Fig. S6). In addition, molecular dynamics simulations were conducted to examine the interaction between MXF-R or DMAPy and lipid membranes. The 1-palmitoyl-2-oleoyl-sn-glycero-3-phosphocholine (POPC) bilayer membrane was constructed to simulate the lipid membrane (Fig. 4A and Fig. S7) and mass density profiles of tail, headgroup and water was shown in Fig. S8. For clarity, the membrane center was defined as Z = 0 Å and symmetrically extended. As the Z value increases from 0 to 40 Å, the lipophilicity gradually changes from hydrophobic to hydrophilic. Next, MXF-R and DMAPy were used to insert into the center of the lipid membrane model, adequately equilibrated, and subsequently analyzed their positions and intermolecular interactions. Fig. 4B and C showed the representational snapshots of MXF-R and DMAPy interacting with the membrane at their global minima. The distribution of the geometric center of MXF-R and DMAPy at different Z-positions was showed in Fig. 4D, which revealed that MXF-R preferably stayed in the lipid membrane for a longer time than that of DMAPy. Moreover, the interaction energy (mainly van der Waals
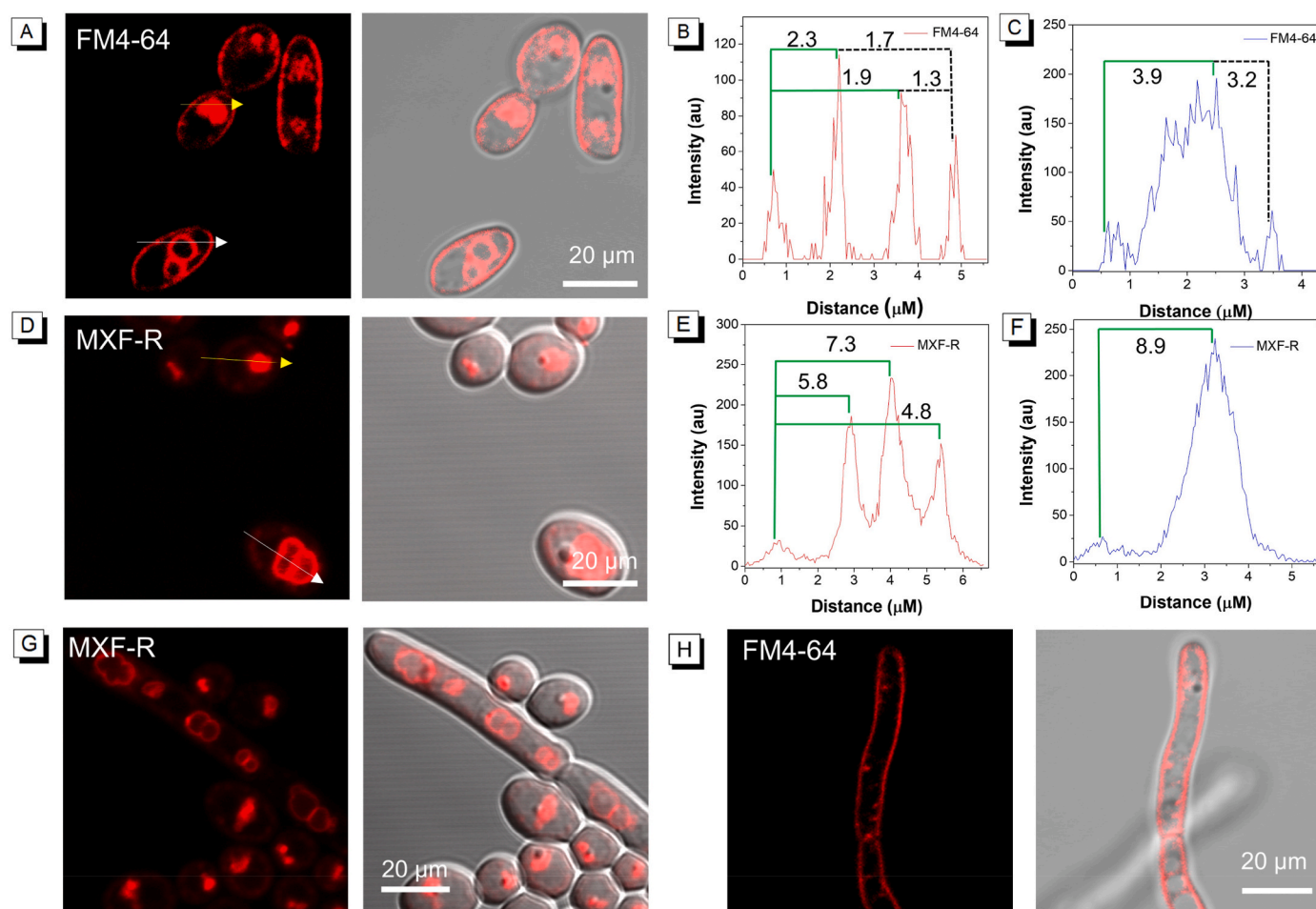

Fig. 3. (A) Photographs of *C. albicans* (yeast morphologies) stained with commercial dye FM4-64 in PBS solution. The intensity profile of synchrony for linear analysis in (B) the white arrow and (C) the yellow arrow in Fig. 3A, respectively. (D) Photographs of *C. albicans* (yeast morphologies) stained with MXF-R in PBS solution. The intensity profile of synchrony for linear analysis in (E) the white arrow and (F) the yellow arrow in Fig. 3D, respectively. Photographs of *C. albicans* (pseudohyphal morphologies) stained with (G) MXF-R and (H) FM4-64 in PBS solution. The concentration of MXF-R was 10 μM. (For interpretation of the references to colour in this figure legend, the reader is referred to the Web version of this article.)
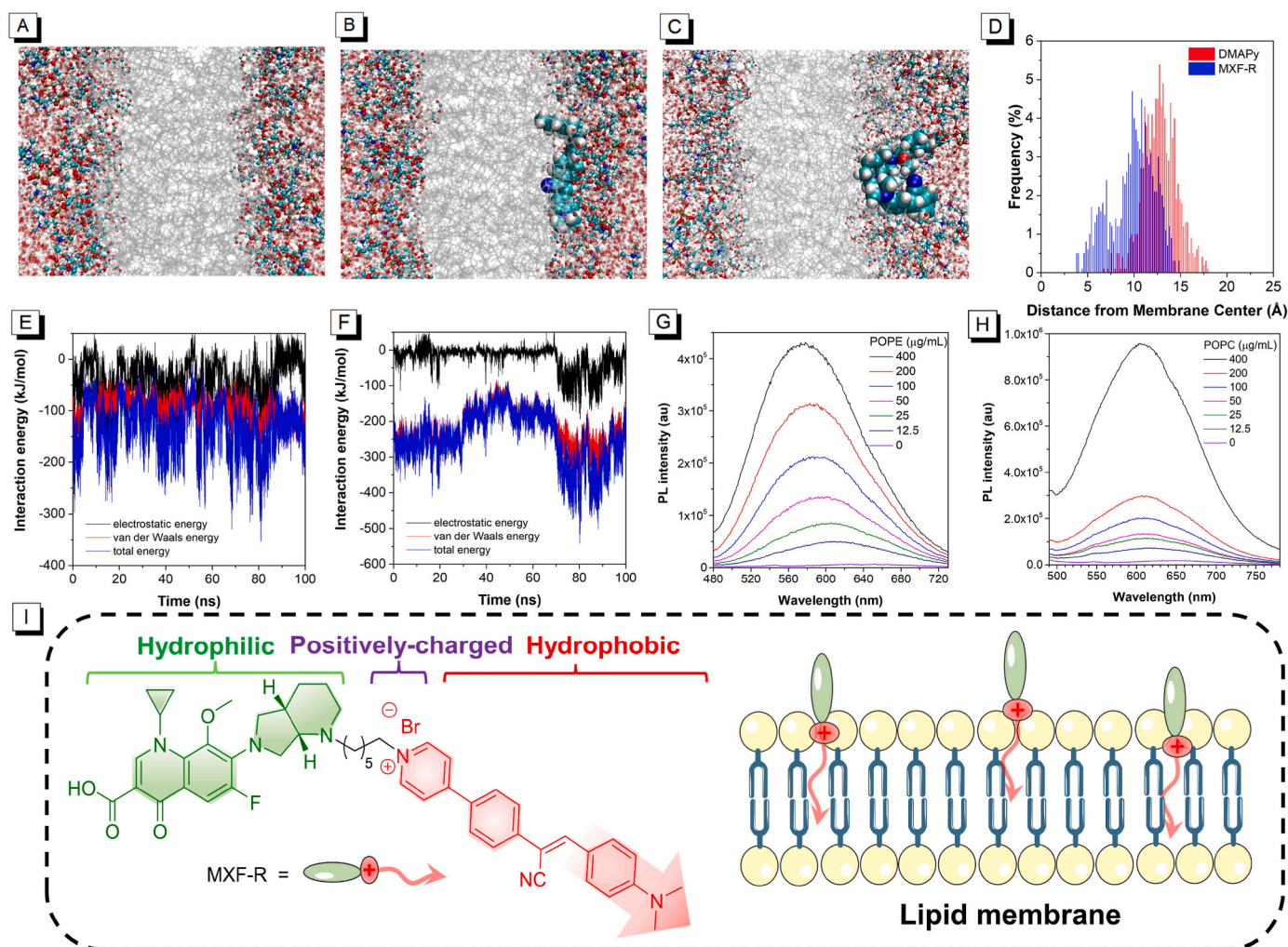
Fig. 4. (A) The simulation model of POPC lipid membrane in water. The simulation model of (B) DMAPy and (C) MXF-R molecules in the POPC lipid bilayers. (D) The distribution of the geometric center of the AIE molecules at different Z-positions within the POPC lipid bilayers. The Coulombic (black), van der Waals (red), and total (blue) interaction energies between (E) DMAPy or (F) MXF-R and the POPC lipid bilayers. PL intensity of MXF-R at different concentrations (G) POPE or (H) POPC, where the concentration of MXF-R was 10 μM. (I) Analysis of hydrophilic and hydrophobic parts of MXF-R and schematic diagram of MXF-R's distribution in the lipid membrane. (For interpretation of the references to colour in this figure legend, the reader is referred to the Web version of this article.)

energy) between the molecules and the POPC lipid bilayers demonstrated that MXF-R had a higher energy through lipid membranes than that of DMAPy (Fig. 4E and F and Fig. S9). This result suggested that MXF-R was relatively difficult to penetrate the membrane.

To further test the membrane-targeting capabilities of MXF-R, cell imaging experiments were performed because the cell membrane and vacuole membrane have similar phospholipid bilayer structure. As shown in Fig. S10, MXF-R remained on the cell membrane for a long time, while DMAPy entered HeLa cells smoothly with the extension of time. This result indicated that MXF-R had better retention ability in the membrane than DMAPy, which was consistent with the theoretical calculation.

Furthermore, the fluorescent co-localization experiment showed that MXF-R highly overlapped with the green plasma membrane stain and the Pearson's correlation coefficient R was 0.86 (Fig. S11). Phosphatidyl ethanolamine (POPE) and 1-palmitoacyl-2-oleyl lecithin (POPC) are the main components of phospholipid bilayer. Therefore, the fluorescence spectra of MXF-R were tested with different concentrations of POPE and POPC. The results showed that with the increase of POPE and POPC, the PL intensity of MXF-R was enhanced obviously and the emission wavelength was blue-shifted (Fig. 4G and H). To sum up, as a positively charged amphiphilic molecule, the hydrophobic portion of MXF-R can be easily inserted into the phospholipid bilayer by the hydrophobic

interaction. Meanwhile, the positive charge of pyridinium electrostatically interacted with phosphoric acid. Notably, because MXF moiety in MXF-R possesses the hydrophilicity and large steric resistance, the resistance of MXF-R through excellent lipid membrane was greatly enhanced. Therefore, MXF-R possessed phospholipid bimolecular targeting ability (Fig. 4I).

3.5. Visualization of fungal vacuole formation

Encouraged by above excellent staining effect of MXF-R on vacuolar membrane of *C. albicans*, we applied it to visualize the formation process of vacuoles, which could help researchers understand how funguses proliferate. First, *C. albicans* stained by MXF-R were cultured in yeast extract peptone dextrose (YPD) medium at 37 °C. Then, the process of fungal vacuole formation was visualized under CLSM. As shown in Fig. 5 and S12, the progeny of *C. albicans* appeared and gradually grew by budding reproduction after incubation for 30 min. Moreover, at 45 min, the red fluorescence signal was detected in the progeny. From 48 to 57 min, the fluorescently-stained substance in the parent generation were gradually transferred to the offsprings. At 60 min, two circular vesicle structures were visualized in the parent *C. albicans* while those fluorescently-stained substances kept transferring. From 66 to 72 min, the translocation of the fluorescently-stained substances was completed
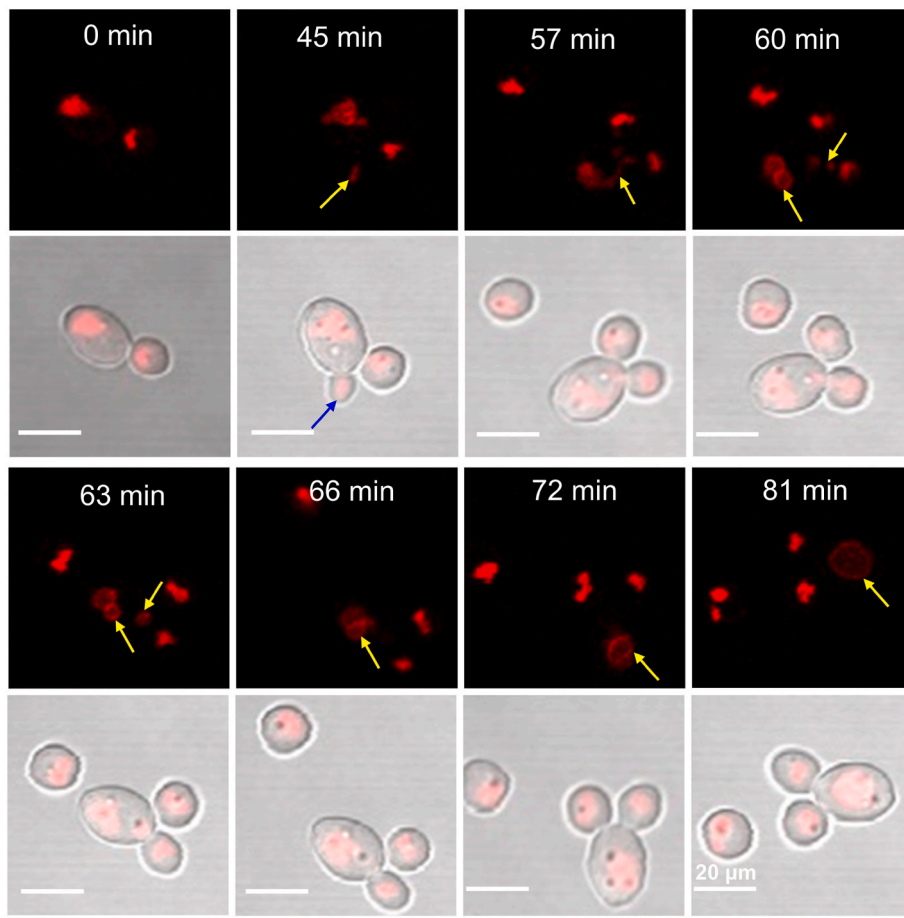
Fig. 5. Fluorescent photographs of the proliferation process of *C. albicans* visualized by MXF-R at 37 °C. The blue arrow indicates the progeny of *C. albicans*. The yellow arrows indicate the transfer of substance during vacuole formation. (For interpretation of the references to colour in this figure legend, the reader is referred to the Web version of this article.)
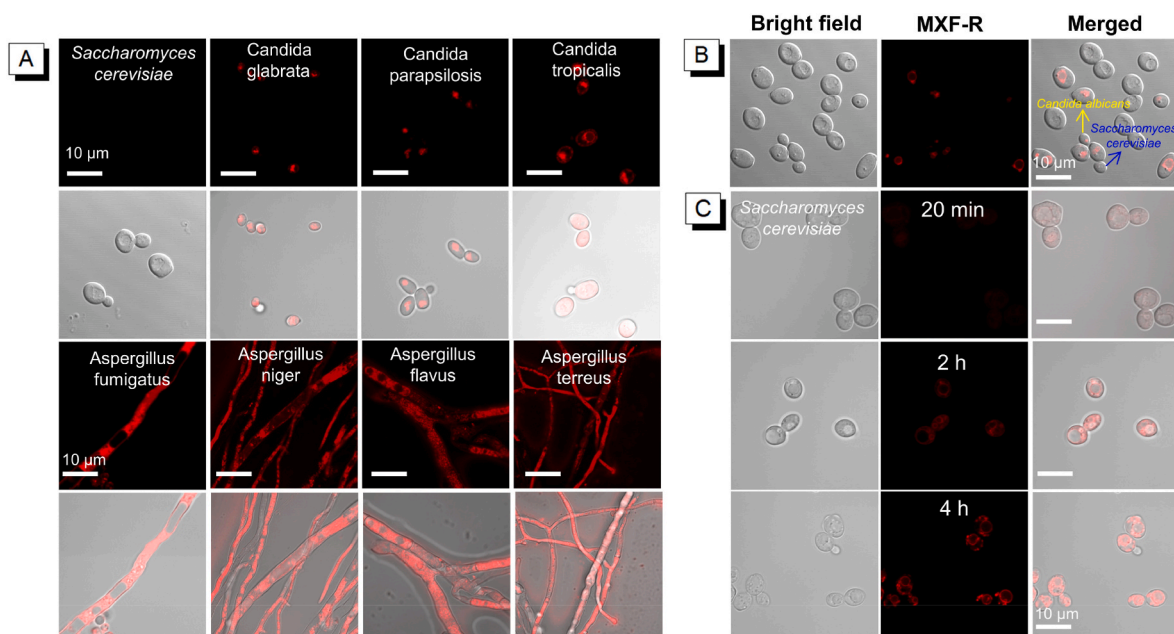

Fig. 6. (A) Fluorescent photographs of different fungal strains stained by MXF-R in PBS solution for 20 min. (B) Fluorescent photographs of mixed strains (*C. albicans* and *S. cerevisiae*) incubated with MXF-R in PBS solution for 20 min. (C) Fluorescent photographs of *S. cerevisiae* incubated with MXF-R in PBS solution with prolonged incubation time. The concentration of MXF-R was 10 μM, $OD_{600} = 0.2$.

and the two vesicles were merged to form a complete vacuole in the parent fungus. Next, the vacuole gradually grew and eventually formed a mature vacuole from 75 to 87 min. In addition, *C. albicans* (yeast, hypha and pseudohyphae) with the different morphologies were stained by MXF-R (Fig. S13). Except for staining on the vacuolar membrane, the fluorescently-stained substance was localized at the anterior end of *hyphal C. albicans*, which was the result of the continuous proliferation of *C. albicans*. Consequently, we inference that the fluorescently-stained substance was passed along with the propagation of hyphal *C. albicans* (Fig. S13). This is the first time to observe the vacuole formation process using fluorescence imaging, demonstrating the capability of MXF-R for in situ visualization of biological proliferation processes.

3.6. Fungal species differentiation

The identification of different fungal species is a prerequisite for effective treatment in clinical treatment. Fluorescence imaging technology has been applied to the identification of different species of microorganisms because of its simple operation, in situ visualization, and rapid detection [37,38]. However, the identification of different types of funguses is very difficult because they possess highly similar morphological structures. To test whether MXF-R has the capability to discriminate different funguses, we used it to stain different fungal species. As shown in Fig. 6A, MXF-R was incubated with different funguses in PBS solutions for 20 min. The results showed that MXF-R was difficult to stain *Saccharomyces cerevisiae* (*S. cerevisiae*). Whereas, MXF-R was mainly distributed in the vacuolar membrane of *Candida tropicalis*, *Candida parapsilosis* and *Candida glabrata*, which were similar to that of *C. albicans*. However, MXF-R mainly entered the interior of the molds (*Aspergillus fumigatus*, *Aspergillus niger*, *Aspergillus flavus* and *Aspergillus terrestris*) without specific targeting. As a sharp contrast, the staining position of DMAPy was mainly in the mitochondria for *S. cerevisiae*, *Candida tropicalis*, *Candida parapsilosis* and *Candida glabrata* without difference (Fig. S14). In addition, the staining of the molds by DMAPy was similar to that of MXF-R (Fig. S15).

Next, we mixed *C. albicans* and *S. cerevisiae* to simulate their symbiotic environment, and then MXF-R was incubated with the mixed fungal sample in PBS solution for 20 min. It was found that MXF-R could specifically recognize and stain *C. albicans*, while no significant fluorescence signal was observed in *S. cerevisiae* (Fig. 6B). It is worth pointing out that the fungi indicated by arrows in Fig. 6B are difficult to distinguish by appearance and morphology (Fig. 6B). Furthermore, the method of fluorescent staining can be quickly and accurately identified.

Next, the reason for the specific staining of *C. albicans* was explored. We hypothesized that this staining difference might be due to the different entering rates of MXF-R. Therefore, we took fluorescent photographs of *S. cerevisiae* with MXF-R at different intervals (Fig. 6C). When incubating for 20 min, MXF-R entered the interior of *S. cerevisiae*, but there was little fluorescence signal on the vacuolar membrane. When the incubation time reached 2 h, MXF-R began to enrich on the vacuolar membrane and fluorescence signals appeared. With incubation time reaching 4 h, the red-emission of MXF-R was found on vacuolar membrane. These results also confirmed MXF-R require relatively longer time to stain the vacuole membrane in *S. cerevisiae* than that of *C. albicans*.

Furthermore, *S. cerevisiae* and *C. albicans* was treated with 75 % ethanol to change the permeability of their plasma membrane. Using the same staining method, it was found that MXF-R rapidly entered these *S. cerevisiae* and was evenly distributed within the fungal cells (Fig. S16A). Notably, MXF-R had lost its ability to target vacuolar membranes in the treated *C. albicans* (Fig. S16B). These results indicated that the survival state of *C. albicans* had a great influence on targeting imaging by MXF-R. In addition, the *C. albicans* stained by MXF-R were fixed with 4 % paraformaldehyde, and the results showed that the MXF-R on the membrane were detached and dispersed within the fungal cells (Fig. S16C). These experiments suggest that MXF-R can only target vacuolar membranes in live fungi.

3.7. Fungi killing by MXF-R

In addition to achieving the differentiation of fungal species, the antifungal effect of MXF-R was investigated. For comparison, FM4-64 and DMAPy were also tested. First, the survival rates of the *C. albicans* stained with FM4-64, DMAPy or MXF-R were investigated by incubating in PBS for 50 min and coating on plates in the absence of light. The results showed that with the increase in the concentration of FM4-64 and DMAPy, the activity of *C. albicans* gradually decreased (Figs. S17 and 18). When the concentrations of FM4-64 and DMAPy were 10 μM, the survival rates of *C. albicans* were 67 % and 37 %, respectively. This antifungal effect possibly due to the positive charge of compounds disrupted the functions of fungus. In contrast, MXF-R had little effect on *C. albicans* at concentrations below 10 μM (Fig. 7A), suggesting that MXF-R possesses a good biocompatibility in dark, thus are suitable for fungal imaging. This effect might be ascribed to the presence of MXF unit in MXF-R that introduces a carboxyl group to partially neutralize positive charge (Fig. S5). Notably, owing to the incorporation of DMAPy derivative as photosensitizing unit, MXF-R could generate ROS upon light irradiation, which could be used to kill *C. albicans*. When the *C. albicans* suspensions were exposed to white light for 30 min in the presence of MXF-R and DMAPy with a concentration of 10 μM for 20 min, the fungi were killed with rates as high as 99.5 % (Fig. 7B and Fig. S18). Furthermore, the therapeutic efficiency of photodynamic therapy (PDT) of MXF-R and DMAPy was compared with the antifungal drug Fluconazole in terms of antifungal activity, and the results indicated that the antifungal effect of Fluconazole was much lower than that of MXF-R and DMAPy with white light irradiation (Fig. S19).

After proving the antifungal effect of MXF-R, its mechanism was studied. DCFH-DA, an indicator of ROS, was used to monitor changes in the content of ROS in *C. albicans* with or without white light irradiation. In the absence of white light, MXF-R-treated *C. albicans* showed no obvious green fluorescence signal from the indicator (Fig. 7C), whereas, upon irradiated by white light for 5 min, a green fluorescence of DCF became stronger. Notably, after the addition of the ROS scavenger of n-acetyl-L-cysteine (NAC), no significant green fluorescence of DCF was detected under white light irradiation (Fig. S20). These findings indicate that the killing of *C. albicans* in the presence of MXF-R is via PDT.

Following, we studied the changes in the distribution of MXF-R and DMAPy in *C. albicans* before and after white light irradiation by fluorescence imaging (Fig. 7D and S21). MXF-R stained the precursors of vacuolar membranes while DMAPy mainly distributed in mitochondria in the absence of white light irradiation. After white light irradiation, MXF-R began to shed from the original stained structure and dispersed whole *C. albicans*. However, the distribution of DMAPy in *C. albicans* was retained in mitochondria. This distribution change indirectly indicated that the vacuolar membrane of *C. albicans* was destroyed by PDT. Moreover, the effect of PDT on the morphology of *C. albicans* was studied through scanning electron microscopy (SEM). After incubating MXF-R with *C. albicans* in PBS for 50 min, the outer membrane of the *C. albicans* remained intact. However, when the system was irradiated by white light for 30 min, the depression of the outer membrane of the *C. albicans* could be clearly observed (Fig. 7E), confirming that MXF-R destroyed the fungal membrane structure to achieve rapid fungi killing. It is worth mentioning that MXF-R shows excellent biocompatibility toward normal L929 cells under both light irradiated and dark conditions as confirmed by the cytotoxicity experiments (Fig. S22). Thanks to its effective species selectivity and potent antifungal properties, MXF-R holds great potential as a diagnostic and therapeutic agent in clinical diseases, such as vaginitis and wound infection caused by candida.

4. Conclusion

In this work, we demonstrated that a biocompatible AIE probe of MXF-R could specifically image *C. albicans* vacuolar membranes, and is
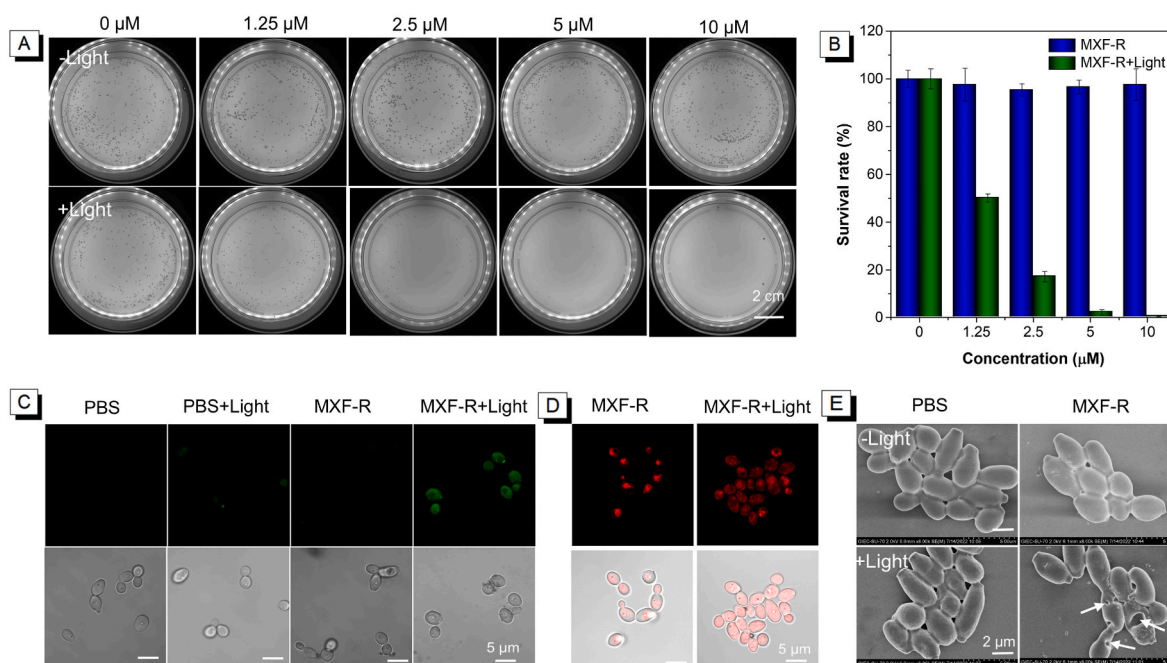
Fig. 7. (A) Killing effects of MXF-R at different concentrations against *C. albicans* with or without white light irradiation (90 mW/cm^2) for 30 min. (B) The survival rate of *C. albicans* treated under different conditions. (C) ROS generation tests using DCFH-DA as an indicator in *C. albicans* cultured MXF-R with or without white light irradiation (90 mW/cm^2) for 5 min. (D) The changes of distribution positions of MXF-R in *C. albicans* before and after white light irradiation. (E) The SEM photos of MXF-R-stained *C. albicans* with or without white light irradiation (90 mW/cm^2) for 30 min.

significantly superior over the commercial probe of FM4-64. More importantly, MXF-R possessed less effect on the activity of *C. albicans* than the positively-charged DMAPy and FM4-64. Thanks to its excellent ability to target vacuolar membranes, MXF-R could in situ trace the vacuole formation process of *C. albicans*, and fluorescently differentiate *C. albicans* and *S. cerevisiae* by taking advantage of their different inner structures. Moreover, the efficient ROS generation ability of MXF-R make it applicable in rapid killing of *C. albicans* by destroying its plasma membrane and vacuolar membrane, and its antifungal effect is better than that of the Fluconazole. Therefore, for the first time, we reported a multifunctional vacuolar membrane probe for vacuole formation visualization, fungal species differentiation and photodynamic killing, which provided a favorable tool for the rapid detection and effective treatment of fungal infections.

CRediT authorship contribution statement

Bingnan Wang: Writing – original draft, Investigation, Formal analysis, Data curation, Conceptualization. **Siyuan Wang:** Writing – original draft, Investigation, Formal analysis, Data curation. **Chunyang Li:** Writing – original draft, Investigation, Formal analysis, Data curation. **Jianqing Li:** Writing – original draft, Investigation, Formal analysis, Data curation. **Meixi Yi:** Writing – original draft, Investigation, Formal analysis, Data curation. **Jing-Wen Lyu:** Writing – original draft, Resources, Investigation, Data curation. **Bing Gu:** Writing – review & editing, Supervision, Resources, Investigation, Data curation. **Ryan T.K. Kwok:** Writing – review & editing, Resources, Investigation, Data curation. **Jacky W.Y. Lam:** Writing – review & editing, Resources, Methodology, Formal analysis. **Anjun Qin:** Writing – review & editing, Supervision, Funding acquisition, Conceptualization. **Ben Zhong Tang:** Writing – review & editing, Supervision, Resources, Project administration, Funding acquisition, Conceptualization.

Declaration of competing interest

The authors declare that they have no known competing financial interests or personal relationships that could have appeared to influence the work reported in this paper.

Appendix A. Supplementary data

Supplementary data to this article can be found online at https://doi.org/10.1016/j.mtbio.2024.101329.

Data availability

Data will be made available on request.

References

[1] G.D. Brown, D.W. Denning, S.M. Levitz, Tackling human fungal infections, Science 336 (2012), https://doi.org/10.1126/science.1222236, 647-647.

[2] D.P. Kontoyiannis, R.E. Lewis, Antifungal drug resistance of pathogenic fungi, Lancet 359 (2002) 1135–1144, https://doi.org/10.1016/S0140-6736(02)08162-X.

[3] A. Goffeau, The fight against fungi, Nature 452 (2008) 541–542, https://doi.org/10.1038/452541a.

[4] X. Didelot, R. Bowden, D.J. Wilson, T.E.A. Peto, D.W. Crook, Transforming clinical microbiology with bacterial genome sequencing, Nat. Rev. Genet. 13 (2012) 601–612, https://doi.org/10.1038/nrg3226.

[5] M.-Y. Wu, X. Xu, R. Hu, Q. Chen, L. Chen, Y. Yuan, J. Li, L. Zhou, S. Feng, L. Wang, S. Chen, M. Gu, A Membrane-targeted photosensitizer prevents drug resistance and

induces immune response in treating candidiasis, Adv. Sci. 10 (2023) 2207736, https://doi.org/10.1002/advs.202207736.

[6] X. Cui, Z. Zhang, Y. Yang, S. Li, C.-S. Lee, Organic radical materials in biomedical applications: state of the art and perspectives, Exploration 2 (2022) 20210264, https://doi.org/10.1002/EXP.20210264.

[7] Q. Liu, X. Chen, Y. Jiang, M. Yan, B. Yu, W. Zhang, Y. Cen, J. Zhang, J. Zhang, Q. Lei, S. Li, B. Yang, Self-promoted targeting delivery of nanodrug through chemotherapeutic upregulation of CD47 for triple begative breast cancer therapy, Adv. Funct. Mater. 34 (2024) 2311677, https://doi.org/10.1002/adfm.202311677.

[8] S.N. Pedro, B.F.A. Valente, C. Vilela, H. Oliveira, A. Almeida, M.G. Freire, A.J. D. Silvestre, C.S.R. Freire, Switchable adhesive films of pullulan loaded with a deep eutectic solvent-curcumin formulation for the photodynamic treatment of drug-resistant skin infections, Mater. Today Bio 22 (2023) 100733, https://doi.org/10.1016/j.mtbio.2023.100733.

[9] K. Zhou, S. Wang, L. Xu, H. Li, Y. Wang, Z. Qiu, G. Zhang, Z. Zhao, B.Z. Tang, AIEgen-based smart system for fungal-infected wound monitoring and on-demand photodynamic therapy, Matter 6 (2023) 3449–3462, https://doi.org/10.1016/j.matt.2023.06.028.

[10] A.C. Sedgwick, K.-C. Yan, D.N. Mangel, Y. Shang, A. Steinbrueck, H.-H. Han, J. T. Brewster, X.-L. Hu, D.W. Snelson, V.M. Lynch, H. Tian, X.-P. He, J.L. Sessler, Deferasirox (ExJade): an FDA-approved AIEgen platform with qnique photophysical properties, J. Am. Chem. Soc. 143 (2021) 1278–1283, https://doi.org/10.1021/jacs.0c11641.

[11] X.-L. Hu, A.C. Sedgwick, D.N. Mangel, Y. Shang, A. Steinbrueck, K.-C. Yan, L. Zhu, D.W. Snelson, S. Sen, C.V. Chau, G. Juarez, V.M. Lynch, X.-P. He, J.L. Sessler, Tuning the solid- and solution-state fluorescence of the iron-chelator deferasirox, J. Am. Chem. Soc. 144 (2022) 7382–7390, https://doi.org/10.1021/jacs.2c01155.

[12] X.-L. Hu, H.-Q. Gan, Z.-Y. Qin, Q. Liu, M. Li, D. Chen, J.L. Sessler, H. Tian, X.-P. He, Phenotyping of methicillin-resistant staphylococcus aureus using a ratiometric sensor array, J. Am. Chem. Soc. 145 (2023) 8917–8926, https://doi.org/10.1021/jacs.2c12798.

[13] P. Sudbery, N. Gow, J. Berman, The distinct morphogenic states of Candida albicans, Trends Microbiol. 12 (2004) 317–324, https://doi.org/10.1016/j.tim.2004.05.008.

[14] M. Uchida, G. McDermott, M. Wetzler, M.A. Le Gros, M. Myllys, C. Knoechel, A. E. Barron, C.A. Larabell, A. Soft X-ray tomography of phenotypic switching and the cellular response to antifungal peptoids in Candida albicans, Proc. Natl. Acad. Sci. 106 (2009) 19375–19380, https://doi.org/10.1073/pnas.0906145106.

[15] J. Li, Z. Meng, Z. Zhuang, B. Wang, J. Dai, G. Feng, X. Lou, F. Xia, Z. Zhao, B. Z. Tang, Effective therapy of drug-resistant bacterial infection by killing planktonic bacteria and destructing biofilms with cationic photosensitizer based on phosphindole oxide, Small 18 (2022) 2200743, https://doi.org/10.1002/smll.202200743.

[16] J. Dai, X. Wu, S. Ding, X. Lou, F. Xia, S. Wang, Y. Hong, Aggregation-induced emission photosensitizers: from molecular design to photodynamic therapy, J. Med. Chem. 63 (2020) 1996–2012, https://doi.org/10.1021/acs.jmedchem.9b02014.

[17] Z. Ye, W. He, Z. Zhang, Z. Qiu, Z. Zhao, B.Z. Tang, AIEgens for microorganism-related visualization and therapy, Interdisc. Med. 1 (2023) e20220011, https://doi.org/10.1002/INMD.20220011.

[18] L. Zheng, Y. Zhu, Y. Sun, S. Xia, S. Duan, B. Yu, J. Li, F.J. Xu, Flexible modulation of cellular activities with cationic photosensitizers: insights of alkyl chain length on reactive oxygen species antimicrobial mechanisms, Adv. Mater. 35 (2023) 2302943, https://doi.org/10.1002/adma.202302943.

[19] C.Y.Y. Yu, H. Xu, S. Ji, R.T.K. Kwok, J.W.Y. Lam, X. Li, S. Krishnan, D. Ding, B. Z. Tang, Mitochondrion-anchoring photosensitizer with aggregation-induced emission characteristics synergistically boosts the radiosensitivity of cancer cells to ionizing radiation, Adv. Mater. 29 (2017) 1606167, https://doi.org/10.1002/adma.201606167.

[20] Q. Liu, T. Pu, X. Zhou, J. Sun, W. Yuan, S. Zhang, M. Zhang, M. Zhang, J. Peng, F. Li, X. Zhang, C. Xu, A follicle-stimulating hormone receptor-targeted near-infrared fluorescent probe for tumor-selective imaging and photothermal therapy, Mater. Today Bio 24 (2024) 100904, https://doi.org/10.1016/j.mtbio.2023.100904.

[21] X. Zheng, D. Wang, W. Xu, S. Cao, Q. Peng, B.Z. Tang, Charge control of fluorescent probes to selectively target the cell membrane or mitochondria: theoretical prediction and experimental validation, Mater. Horiz. 6 (2019) 2016–2023, https://doi.org/10.1039/C9MH00906J.

[22] Y. Zhang, Q. Wang, Z. Zhu, W. Zhao, C. Yan, Z. Liu, M. Liu, X. Zhao, H. Tian, W.-H. Zhu, Spatiotemporal visualization of cell membrane with amphiphilic aggregation-induced emission-active sensor, CCS Chem. 4 (2022) 1619–1632, https://doi.org/10.31635/ccschem.021.202100967.

[23] Q. Sun, Q. Su, Y. Gao, K. Zhou, W. Song, P. Quan, X. Yang, Z. Ge, Y. Zhang, G. He, Cationic telluroviologen derivatives as type-I photosensitizers for tumor photodynamic theranostics, Aggregate 4 (2023) e298, https://doi.org/10.1002/agt2.298.

[24] G. Zhang, X. Fu, D. Zhou, R. Hu, A. Qin, B.Z. Tang, Smart aggregation-induced emission polymers: preparation, properties and bio-applications, Smart Molecules 1 (2023) e20220008, https://doi.org/10.1002/smo.20220008.

[25] X. Xiao, H. Cai, Q. Huang, B. Wang, X. Wang, Q. Luo, Y. Li, H. Zhang, Q. Gong, X. Ma, Z. Gu, K. Luo, Polymeric dual-modal imaging nanoprobe with two-photon aggregation-induced emission for fluorescence imaging and gadolinium-chelation for magnetic resonance imaging, Bioact. Mater. 19 (2023) 538–549, https://doi.org/10.1016/j.bioactmat.2022.04.026.

[26] T.A. Vida, S.D. Emr, A new vital stain for visualizing vacuolar membrane dynamics and endocytosis in yeast, J. Cell Biol. 128 (1995) 779–792, https://doi.org/10.1083/jcb.128.5.779.

[27] W. Wang, Z. Hu, Targeting peptide-based probes for molecular imaging and diagnosis, Adv. Mater. 31 (2019) 1804827, https://doi.org/10.1002/adma.201804827.

[28] L. Huang, Y. Zhou, D. Jiao, J. Ren, Y. Qi, H. Wang, Y. Shi, D. Ding, X. Xue, Mitochondrial sensitive probe with aggregation-induced emission characteristics for early brain diagnosis of Parkinson's disease, Aggregate 5 (2024) e403, https://doi.org/10.1002/agt2.403.

[29] X. Xue, Y. Zhao, L. Dai, X. Zhang, X. Hao, C. Zhang, S. Huo, J. Liu, C. Liu, A. Kumar, W.-Q. Chen, G. Zou, X.-J. Liang, Spatiotemporal drug release visualized through a drug delivery system with tunable aggregation-induced emission, Adv. Mater. 26 (2014) 712–717, https://doi.org/10.1002/adma.201302365.

[30] B. Wang, L. Wang, X. Wu, X. Liu, J. Zhu, R. Hu, D. Ding, A. Qin, B.Z. Tang, The commercial antibiotics with inherent AIE feature: in situ visualization of antibiotic metabolism and specifically differentiation of bacterial species and broad-spectrum therapy, Bioact. Mater. 23 (2023) 223–233, https://doi.org/10.1016/j.bioactmat.2022.11.002.

[31] Y. Chen, P. Pei, Y. Yang, H. Zhang, F. Zhang, Noninvasive early diagnosis of allograft rejection by a granzyme B protease responsive NIR-II bioimaging nanosensor, Angew. Chem. Int. Ed. 62 (2023) e202301696, https://doi.org/10.1016/j.bioactmat.2022.11.002.

[32] T. Zhou, R. Hu, L. Wang, Y. Qiu, G. Zhang, Q. Deng, H. Zhang, P. Yin, B. Situ, C. Zhan, A. Qin, B.Z. Tang, An AIE-active conjugated polymer with high ROS-generation ability and biocompatibility for efficient photodynamic therapy of bacterial infections, Angew. Chem. Int. Ed. 59 (2020) 9952–9956, https://doi.org/10.1002/anie.201916704.

[33] B. Wang, S. Liu, X. Liu, R. Hu, A. Qin, B.Z. Tang, Aggregation-induced emission materials that aid in pharmaceutical research, Adv. Healthcare Mater. 10 (2021) 2101067, https://doi.org/10.1002/adhm.202101067.

[34] R. Hu, F. Zhou, T. Zhou, J. Shen, Z. Wang, Z. Zhao, A. Qin, B.Z. Tang, Specific discrimination of gram-positive bacteria and direct visualization of its infection towards mammalian cells by a DPAN-based AIEgen, Biomaterials 187 (2018) 47–54, https://doi.org/10.1016/j.biomaterials.2018.09.019.

[35] B. Wang, L. Wang, X. Liu, J. Zhu, R. Hu, A. Qin, B.Z. Tang, AIE-active antibiotic photosensitizer with enhanced fluorescence in bacteria infected cells and better therapy effect toward drug-resistant bacteria, ACS Appl. Bio Mater. 5 (2022) 4955–4964, https://doi.org/10.1021/acsabm.2c00681.

[36] A. Jadhav, B. Bansode, D. Phule, A. Shelar, R. Patil, W. Gade, K. Kharat, S. M. Karuppayil, The antibacterial agent, moxifloxacin inhibits virulence factors of Candida albicans through multitargeting, World J. Microbiol. Biotechnol. 33 (2017) 96, https://doi.org/10.1007/s11274-017-2264-z.

[37] C. Zhou, W. Xu, P. Zhang, M. Jiang, Y. Chen, R.T.K. Kwok, M.M.S. Lee, G. Shan, R. Qi, X. Zhou, J.W.Y. Lam, S. Wang, B.Z. Tang, Engineering sensor arrays using aggregation-induced emission luminogens for pathogen identification, Adv. Funct. Mater. 29 (2019) 1805986, https://doi.org/10.1002/adfm.201805986.

[38] C. Zhou, W. Jiang, J. Du, H. Bai, G. Shan, R.T.K. Kwok, J.H.C. Chau, J. Zhang, J.W. Y. Lam, P. Huang, B.Z. Tang, One stone, three birds: one AIEgen with three colors for fast differentiation of three pathogens, Chem. Sci. 11 (2020) 4730–4740, https://doi.org/10.1039/D0SC00256A.